Analytical study of pulse amplification in silicon Raman amplifiers

Ivan D. Rukhlenko,[1,*] Malin Premaratne,[1] Ivan L. Garanovich,[2] Andrey A. Sukhorukov,[2] and Govind P. Agrawal[3]

[1]*Advanced Computing and Simulation Laboratory (AχL), Department of Electrical and Computer Systems Engineering, Monash University, Clayton, VIC 3800, Australia*
[2]*Nonlinear Physics Centre, Research School of Physics and Engineering, The Australian National University, Canberra, ACT 0200, Australia*
[3]*Institute of Optics, University of Rochester, Rochester, NY 14627, USA*
[*]*ivan.rukhlenko@monash.edu*

Abstract: The nonlinear process of stimulated Raman scattering is important for silicon photonics as it enables optical amplification and lasing. To understand the dynamics of silicon Raman amplifiers (SRAs), a numerical approach is generally employed, even though it provides little insight into the contribution of different SRA parameters to the signal amplification process. In this paper, we solve the coupled pump–signal equations analytically under realistic conditions, and derive an exact formula for the envelope of a signal pulse when picosecond optical pulses are amplified inside a SRA pumped by a continuous-wave laser beam. Our solution is valid for an arbitrary pulse shape and fully accounts for the Raman gain-dispersion effects, including temporal broadening and group-velocity reduction (a slow-light effect). It can be applied to any pumping scenario and leads to a simple analytic expression for the maximum optical delay produced by the Raman dispersion in a unidirectionally pumped SRA. We employ our analytical formulation to study the evolution of optical pulses with Gaussian, exponential, and Lorentzian shapes. The ability of a Gaussian pulse to maintain its shape through the amplifier makes it possible to realize soliton-like propagation of chirped Gaussian pulses in SRAs. We obtain analytical expressions for the required linear chirp and temporal width of a soliton-like pulse in terms of the net signal gain and the Raman-dispersion parameter. Our results are useful for optimizing the performance of SRAs and for engineering controllable signal delays.

OCIS codes: (040.6040) Silicon; (190.5650) Raman effect; (250.4390) Nonlinear optics, integrated optics; (230.1150) All-optical devices; (999.9999) Slow light.

References and links

1. R. A. Soref, "The past, present, and future of silicon photonics," IEEE J. Sel. Top. Quantum Electron. **12**, 1678–1687 (2006).
2. B. Jalali, O. Boyraz, V. Raghunathan, D. Dimitropoulos, and P. Koonath, "Silicon Raman amplifiers, lasers and their applications," in *Active and Passive Optical Components for WDM Communications V*, A. K. Dutta, Y. Ohishi, N. K. Dutta, and J. Moerk, Eds., Proc. SPIE **6014**, 21–26 (2005).
3. G. T. Reed and A. P. Knights, *Silicon Photonics: An Introduction* (Wiley, Hoboken, 2004).
4. H. K. Tsang and Y. Liu, "Nonlinear optical properties of silicon waveguides," Semicond. Sci. Technol. **23**, 064007(1–9) (2008).

#131277 - $15.00 USD Received 7 Jul 2010; revised 11 Aug 2010; accepted 11 Aug 2010; published 12 Aug 2010

5. B. Jalali, V. Raghunathan, D. Dimitropoulos, and O. Boyraz, "Raman-based silicon photonics," IEEE J. Sel. Top. Quantum Electron. **12**, 412–421 (2006).
6. M. Dinu, F. Quochi, and H. Garcia, "Third-order nonlinearities in silicon at telecom wavelengths," Appl. Phys. Lett. **82**, 2954–2956 (2003).
7. I-W. Hsieh, X. Chen, J. I. Dadap, N. C. Panoiu, and R. M. Osgood, Jr., "Cross-phase modulation-induced spectral and temporal effects on co-propagating femtosecond pulses in silicon photonic wires," Opt. Express **15**, 1135–1146 (2007).
8. I-W. Hsieh, X. Chen, X. Liu, J. I. Dadap, N. C. Panoiu, C. Y. Chou, F. Xia, W. M. Green, Y. A. Vlasov, and R. M. Osgood, Jr., "Supercontinuum generation in silicon photonic wires," Opt. Express **15**, 15242–15249 (2007).
9. E. K. Tien, N. S. Yuksek, F. Qian, and O. Boyraz, "Pulse compression and modelocking by using TPA in silicon waveguides," Opt. Express **15**, 6500–6506 (2007).
10. R. Dekker, A. Driessen, T. Wahlbrink, C. Moormann, J. Niehusmann, and M. Först, "Ultrafast Kerr-induced all-optical wavelength conversion in silicon waveguides using 1.55 μm femtosecond pulses," Opt. Express **14**, 8336–8346 (2006).
11. E. Dulkeith, Y. A. Vlasov, X. Chen, N. C. Panoiu, and R. M. Osgood, Jr., "Self-phase-modulation in submicron silicon-on-insulator photonic wires," Opt. Express **14**, 5524–5534 (2006).
12. T. Liang, L. Nunes, T. Sakamoto, K. Sasagawa, T. Kawanishi, M. Tsuchiya, G. Priem, D. V. Thourhout, P. Dumon, R. Baets, and H. Tsang, "Ultrafast all-optical switching by cross-absorption modulation in silicon wire waveguides," Opt. Express **13**, 7298–7303 (2005).
13. O. Boyraz, T. Indukuri, and B. Jalali, "Self-phase-modulation induced spectral broadening in silicon waveguides," Opt. Express **12**, 829–834 (2004).
14. R. Espinola, J. Dadap, R. Osgood, S. J. McNab, and Y. A. Vlasov, "Raman amplification in ultrasmall silicon-on-insulator wire waveguides," Opt. Express **12**, 3713–3718 (2004).
15. G. P. Agrawal, *Nonlinear Fiber Optics*, 4th ed. (Academic, Boston, 2007).
16. I. D. Rukhlenko, M. Premaratne, and G. P. Agrawal, "Analytical study of optical bistability in silicon ring resonators," Opt. Lett. **35**, 55–57 (2009).
17. L. Yin, J. Zhang, P. M. Fauchet, and G. P. Agrawal, "Optical switching using nonlinear polarization rotation inside silicon waveguides," Opt. Lett. **34**, 476–478 (2009).
18. Q. Lin, O. J. Painter, and G. P. Agrawal, "Nonlinear optical phenomena in silicon waveguides: Modeling and applications," Opt. Express **15**, 16604–16644 (2007).
19. X. Chen, N. C. Panoiu, and R. M. Osgood, "Theory of Raman-mediated pulsed amplification in silicon-wire waveguides," IEEE J. Quantum Electron. **42**, 160–170 (2006).
20. O. Boyraz and B. Jalali, "Demonstration of directly modulated silicon Raman laser," Opt. Express **13**, 796–800 (2005).
21. H. Rong, R. Jones, A. Liu, O. Cohen, D. Hak, A. Fang, and M. Pannicia, "A continuous-wave Raman silicon laser," Nature **433**, 725–728 (2005).
22. R. Jones, A. Liu, H. Rong, M. Paniccia, O. Cohen, and D. Hak, "Lossless optical modulation in a silicon waveguide using stimulated Raman scattering," Opt. Express **13**, 1716–1723 (2005).
23. T. K. Liang and H. K. Tsang, "Nonlinear absorption and Raman scattering in silicon-on-insulator optical waveguides," IEEE J. Sel. Top. Quantum Electron. **10**, 1149–1153 (2004).
24. O. Boyraz and B. Jalali, "Demonstration of a silicon Raman laser," Opt. Express **12**, 5269–5273 (2004).
25. D. Dimitropoulos, B. Houshmand, R. Claps, and B. Jalali, "Coupled-mode theory of Raman effect in silicon-on-insulator waveguides," Opt. Lett. **28**, 1954–1956 (2003).
26. R. Jones, H. Rong, A. Liu, A. W. Fang, M. J. Paniccia, D. Hak, and O. Cohen, "Net continuous-wave optical gain in a low loss silicon-on-insulator waveguide by stimulated Raman scattering," Opt. Express **13**, 519–525 (2005).
27. O. Boyraz and B. Jalali, "Demonstration of 11 dB fiber-to-fiber gain in a silicon Raman amplifier," IEICE Electron. Exp. **1**, 429–434 (2004).
28. A. Liu, H. Rong, M. Paniccia, O. Cohen, and D. Hak, "Net optical gain in a low loss silicon-on-insulator waveguide by stimulated Raman scattering," Opt. Express **12**, 4261–4268 (2004).
29. R. Claps, D. Dimitropoulos, V. Raghunathan, Y. Han, and B. Jalali, "Observation of stimulated Raman amplification in silicon waveguides," Opt. Express **11**, 1731–1739 (2003).
30. R. Claps, D. Dimitropoulos, and B. Jalali, "Stimulated Raman scattering in silicon waveguides," Electron. Lett. **38**, 1352–1354 (2002).
31. I. D. Rukhlenko, C. Dissanayake, M. Premaratne, and G. P. Agrawal, "Optimization of Raman amplification in silicon waveguides with finite facet reflectivities," IEEE J. Sel. Top. Quantum Electron. **16**, 226–233 (2010).
32. I. D. Rukhlenko, M. Premaratne, C. Dissanayake, and G. P. Agrawal, "Continuous-wave Raman amplification in silicon waveguides: Beyond the undepleted pump approximation," Opt. Lett. **34**, 536–538 (2009).
33. I. D. Rukhlenko, C. Dissanayake, M. Premaratne, and G. P. Agrawal, "Maximization of net optical gain in silicon-waveguide Raman amplifiers," Opt. Express **17**, 5807–5814 (2009).
34. M. Krause, H. Renner, and E. Brinkmeyer, "Efficient Raman lasing in tapered silicon waveguides," Spectroscopy **21**, 26–32 (2006).
35. H. Renner, M. Krause, and E. Brinkmeyer, "Maximal gain and optimal taper design for Raman amplifiers in

#131277 - $15.00 USD Received 7 Jul 2010; revised 11 Aug 2010; accepted 11 Aug 2010; published 12 Aug 2010

silicon-on-insulator waveguides," in *Integrated Photonics Research and Applications Topical Meetings* (IPRA 2005), paper JWA3.
36. M. Krause, H. Renner, and E. Brinkmeyer, "Efficiency increase of silicon-on-insulator Raman lasers by reduction of free-carrier absorption in tapered waveguides," in *Conference on Lasers and Electro-Optics* (CLEO 2005), paper CThB1.
37. M. Krause, H. Renner, and E. Brinkmeyer, "Analysis of Raman lasing characteristics in silicon-on-insulator waveguides," Opt. Express **12**, 5703–5710 (2004).
38. S. Roy, S. K. Bhadra, and G. P. Agrawal, "Raman amplification of optical pulses in silicon waveguides: Effects of finite gain bandwidth, pulse width, and chirp," J. Opt. Soc. Am. B **26**, 17–25 (2009).
39. W. Ding, C. Benton, A. V. Gorbach, W. J. Wadsworth, J. C. Knight, D. V. Skryabin, M. Gnan, M. Sorrel, and R. M. De La Rue, "Solitons and spectral broadening in long silicon-on-insulator photonic wires," Opt. Express **16**, 3310–3319 (2008).
40. V. M. N. Passaro and F. D. Leonardis, "Solitons in SOI optical waveguides," Adv. Studies Theor. Phys. **2**, 769–785 (2008).
41. L. Yin, Q. Lin, and G. P. Agrawal, "Soliton fission and supercontinuum generation in silicon waveguides," Opt. Lett. **32**, 391–393 (2007).
42. J. Zhang, Q. Lin, G. Piredda, R. W. Boyd, G. P. Agrawal, and P. M. Fauchet, "Optical solitons in a silicon waveguide," Opt. Express **15**, 7682–7688 (2007).
43. L. Yin, Q. Lin, and G. P. Agrawal, "Dispersion tailoring and soliton propagation in silicon waveguides," Opt. Lett. **31**, 1295–1297 (2006).
44. I. D. Rukhlenko, M. Premaratne, and G. P. Agrawal, "Nonlinear silicon photonics: Analytical tools," IEEE J. Sel. Top. Quantum Electron. **16**, 200–215 (2010).
45. Y. Okawachi, M. A. Foster, J. E. Sharping, A. L. Gaeta, Q. Xu, and M. Lipson, "All-optical slow-light on a photonic chip," Opt. Express **14**, 2317–2322 (2006).
46. I. D. Rukhlenko, M. Premaratne, and G. P. Agrawal, "Analytical study of optical bistability in silicon-waveguide resonators," Opt. Express **17**, 22124–22137 (2009).
47. A. D. Polyanin, *Handbook of Linear Partial Differential Equations for Engineers and Scientists*, (Chapman & Hall/CRC, Boca Raton, 2002).
48. I. D. Rukhlenko, I. Udagedara, M. Premaratne, and G. P. Agrawal, "Effect of free carriers on pump-to-signal noise transfer in silicon Raman amplifiers," Opt. Lett. **35**, 2343–2345 (2010).
49. R. Claps, D. Dimitropoulos, V. Raghunathan, Y. Han, and B. Jalali, "Observation of Raman emission in silicon waveguides at 1.54 μm," Opt. Express **10**, 1305–1313 (2002).

1. Introduction

Despite inherent nonlinear losses, which at high optical powers can diminish the advantages offered by silicon-on-insulator (SOI) technology, SOI waveguides hold strong potential for applications in future telecommunication industry [1–3]. The high refractive index of silicon (3.5 versus 1.5 in fused silica) and its large third-order nonlinearities are the main reasons behind the SOI platform being a promising candidate for on-chip optoelectronic integration [4–6]. An important point is that the strong localization of the optical field reduces the power required for manifestation of the nonlinear effects inside an SOI waveguide. Indeed, only a few centimeters of propagation through a silicon waveguide are required for two optical beams to change their spectra, energy, phase, and polarization owing to stimulated Raman scattering (SRS), self-phase modulation (SPM), cross-phase modulation (XPM), and free-carrier effects [7–14]. To better understand the advantages of silicon over fused silica for all-optical signal processing, it is worth comparing the efficiency of the Kerr and Raman effects in these two media.

The relative efficiency of the third-order nonlinear processes in silicon waveguides and optical fibers can be estimated by multiplying the ratio of the corresponding nonlinear coefficients by a nonlinear reduction factor (NRF), which characterizes the attenuation of nonlinear effects in silicon as compared to silica glass. We define the NRF as the ratio of the intensity integrals for two beams of equal powers propagating through a silicon waveguide and an optical fiber [15],

#131277 - $15.00 USD Received 7 Jul 2010; revised 11 Aug 2010; accepted 11 Aug 2010; published 12 Aug 2010

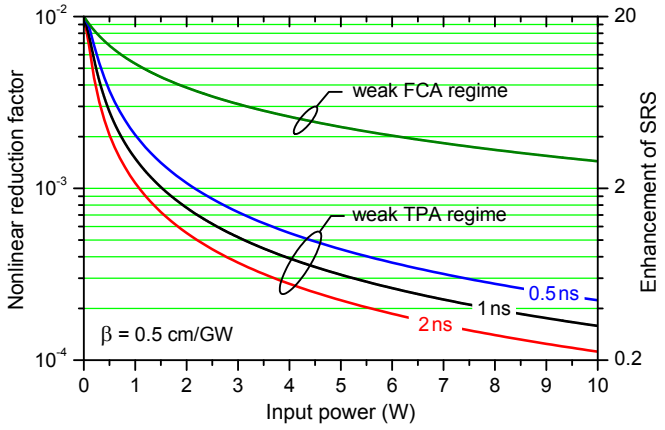

Fig. 1. Nonlinear reduction factor (NRF) as a function of input power for typical silicon waveguides compared to optical fibers. As the free-carrier lifetime is reduced, NRF increases and approaches the limit determined by TPA (top curve). The right scale shows the enhancement of SRS efficiency in silicon waveguides over silica fibers, obtained by multiplying NRF with the ratio of the Raman gain coefficients for silicon and silica (taken to be 2000).

i.e., NRF $= \mathscr{I}_{\rm Si}/\mathscr{I}_{\rm f}$, where 'f' stands for fiber,

$$\mathscr{I}_j = \lim_{L\gg\alpha_j^{-1}} \int_0^L I_j(z)\,{\rm d}z \quad (j = \text{Si or f}),$$

α_j is the linear loss coefficient, and L is the propagation distance. Since the optical intensity decays exponentially inside fibers, $\mathscr{I}_{\rm f}$ is proportional to the incident intensity, $\mathscr{I}_{\rm f} = P/(A_{\rm f}\alpha_{\rm f})$, where P is the input power and $A_{\rm f}$ is the mode area [15].

A more complex picture occurs in silicon waveguides, where the dominant mechanism of optical losses depends on the local field intensity. At high incident powers, free-carrier absorption (FCA) is stronger than two-photon absorption (TPA) and linear losses, near the waveguide input. As the signal intensity decays with propagation, FCA weakens and either TPA or linear loss starts to dominate. Assuming that nonlinear losses are higher than the linear ones, the results of Refs. [16–18] yield the following functional form for $\mathscr{I}_{\rm Si}$:

$$\mathscr{I}_{\rm Si} = \begin{cases} \left(\dfrac{4\pi\hbar c}{\sigma\tau\beta\lambda\alpha_{\rm Si}}\right)^{1/2} \tan^{-1}\left[\left(\dfrac{\sigma\tau\beta\lambda}{4\pi\hbar c\alpha_{\rm Si}}\right)^{1/2}\dfrac{P}{A_{\rm Si}}\right] & \text{in the weak TPA regime,} \\ \dfrac{1}{\beta}\ln\left(1+\dfrac{\beta}{\alpha_{\rm Si}}\dfrac{P}{A_{\rm Si}}\right) & \text{in the weak FCA regime,} \end{cases}$$

where $A_{\rm Si}$ is the effective mode area, τ is the effective free-carrier lifetime, β is the TPA coefficient, λ is the wavelength, and $\sigma = 1.45\times10^{-21}\,{\rm m}^2$. Figure 1 shows NRF for the typical values $\alpha_{\rm f} = 1$ dB/km, $A_{\rm f} = 100\ \mu{\rm m}^2$, $\alpha_{\rm Si} = 1$ dB/cm, $A_{\rm Si} = 0.1\ \mu{\rm m}^2$, and $\lambda = 1.55\ \mu$m. One can see that nonlinear effects in an optical fiber would be much more intense compared with a silicon waveguide if their nonlinear coefficients were the same. This is a consequence of the absence of nonlinear absorption in silica fibers. In the case of silicon waveguides, NRF decreases owing to a sharp rise in TPA and FCA as the input power is increased. Fortunately, the Kerr and Raman coefficients in silicon are, respectively, more than 100 and 2000 times larger than those

#131277 - $15.00 USD Received 7 Jul 2010; revised 11 Aug 2010; accepted 11 Aug 2010; published 12 Aug 2010

in optical fibers. Therefore, at power levels below 1 W, the Kerr-related phenomena are almost equally pronounced in cm-long SOI waveguides and km-long optical fibers. The situation is even better for SRS in SOI waveguides (see the right scale in Fig. 1).

SRS in silicon has been studied extensively in recent years [19–25], after it was found to be capable of producing a net optical gain [26–30]. Continuous-wave (CW) Raman amplification and lasing have received considerable theoretical attention [31–37], because of their relatively simpler description compared with nonstationary problems. In the case of pulses, the overwhelming majority of studies rely on numerical methods, which hinder comprehension of the underlying processes and also make it difficult to generalize the results. A remarkable exception to this statement is the work of Roy *et al.* [38], who used an elegant semi-analytical method to analyze the amplification of signal pulses by a CW pump, and with this were able to reach a number of valuable general conclusions.

In this paper we derive, for the first time to the best of our knowledge, an analytical solution that describes Raman amplification of an *arbitrary* optical pulse in silicon waveguides under CW pumping. The solution takes into consideration the finite width of the Raman gain spectrum and accounts for the related slow down of the pulse resulting from the SRS-induced changes in its group velocity. The structure of the solution allows one to easily analyze the amplification process under different pumping geometries, including the situation of bidirectional pumping. For pulses of specific shapes, analytical expressions describing the evolution of their envelopes can be obtained from the general solution. We derive such expressions for optical pulses with Gaussian, exponential, and Lorentzian profiles. It is well known that, due to large optical losses, silicon waveguides do not support temporal solitons in the ordinary sense [39–43]. We show in this paper how a chirped Gaussian pulse can completely restore its intensity profile after passing through a silicon Raman amplifier.

2. Exact analytical solution of pulse propagation in silicon Raman amplifiers

2.1. Propagation equation for the signal pulse being amplified

Consider amplification of a signal pulse with carrier frequency ω_s, passing through a silicon waveguide, pumped by a CW laser beam at frequency ω_p. In many practical situations, the pump is not depleted much by the signal pulse, and we can assume its intensity I_p to remain time-independent. In this approximation, the equation for the Fourier-transformed signal envelope $\tilde{A}_s(z,\omega-\omega_s)$ has the form [38, 44]

$$\frac{1}{\tilde{A}_s}\frac{\partial\tilde{A}_s}{\partial z}-i\beta_{1s}\omega-i\beta_{2s}\frac{\omega^2}{2}=-\frac{\alpha_s}{2}-(\beta_s+2i\gamma_s)I_p(z)-\left(\frac{\xi_r}{2}+i\xi_i\right)I_p^2(z)+G_R(\omega)I_p(z), \quad (1)$$

where β_{1s} and β_{2s} are the first-order and second-order dispersion parameters; α_s and β_s are the linear-loss and TPA coefficients; $\gamma_s=(\omega_s/c)\,n_2$, $n_2=6\times10^{-5}$ cm^2/GW is the nonlinear Kerr parameter, and c is the speed of light in vacuum. The FCA parameter ξ_r and the free-carrier dispersion (FCD) parameter ξ_i are related to the effective free-carrier lifetime τ_c and the TPA coefficient β_p at the pump frequency as

$$\xi_r=\sigma_r(\omega_0/\omega_s)^2\tau_c\beta_p/(2\hbar\omega_p),\quad \xi_i=(\sigma_i/\sigma_r)(\omega_s/c)\xi_r,\quad \omega_0=2\pi c/(1.55\,\mu\text{m}),$$
$$\sigma_r=1.45\times10^{-21}\,\text{m}^2,\quad \sigma_i=5.3\times10^{-27}\,\text{m}^3.$$

The first three terms on the right side of Eq. (1) represent linear absorption, non-resonant third-order effects of cross-TPA and cross-phase modulation (XPM), and the free-carrier effects. The last term accounts for SRS characterized by the gain spectrum [18]

$$G_R(\omega)=\frac{g_R}{2}\frac{\omega_s}{\omega_p}\frac{\Omega_R}{\Omega_0}\left[\frac{\gamma_R}{\gamma_R-i(\omega-\Omega_{ps}+\Omega_0)}-\frac{\gamma_R}{\gamma_R-i(\omega-\Omega_{ps}-\Omega_0)}\right], \quad (2)$$

#131277 - $15.00 USD Received 7 Jul 2010; revised 11 Aug 2010; accepted 11 Aug 2010; published 12 Aug 2010

where $g_R = 20$ cm/GW is the Raman gain coefficient, $\Omega_R = 15.6$ THz is the Raman shift, $\Omega_0 = (\Omega_R^2 - \gamma_R^2)^{1/2}$, $2\gamma_R \approx 106$ GHz is the full width at half maximum (FWHM) of the Raman gain spectrum, and $\Omega_{ps} = \omega_p - \omega_s > 0$.

In practice, the difference between the pump and signal frequencies is so close to $\Omega_R \approx \Omega_0$ that the first term in the square brackets in Eq. (2) dominates, and the second term can be neglected. In this case, propagation of the signal is governed by the effective dispersion parameters

$$\beta_{1s}^{\text{eff}}(I_p,\omega_p) = \beta_{1s} - iI_p(z)\left.\frac{\mathrm{d}G_R}{\mathrm{d}\omega}\right|_{\omega=0} \approx \beta_{1s} + \frac{\hat{g}_R}{2}\frac{\gamma_R}{[\gamma_R + i(\Omega_{ps}-\Omega_R)]^2}I_p(z),$$
$$\beta_{2s}^{\text{eff}}(I_p,\omega_p) = \beta_{2s} - iI_p(z)\left.\frac{\mathrm{d}^2G_R}{\mathrm{d}\omega^2}\right|_{\omega=0} \approx \beta_{2s} - i\hat{g}_R\frac{\gamma_R}{[\gamma_R + i(\Omega_{ps}-\Omega_R)]^3}I_p(z),$$

where $\hat{g}_R = (\omega_s/\omega_p)g_R$. These expressions show that, when $|\Omega_{ps} - \Omega_R| \lesssim \gamma_R$, the inclusion of Raman dispersion leads to a reduction in the group velocity of the signal and a decrease in Raman gain. The extent of these changes is proportional to the intensity of the pump and depends on the pump frequency. This feature allows one to tune the frequency of the maximal group delay within the signal bandwidth by changing ω_p, and to control the delay time by varying pump intensity [45].

The amplification of sufficiently long optical pulses with maximum efficiency occurring at $\Omega_{ps} = \Omega_R$ deserves further consideration. Assuming that the temporal width of the signal pulse is larger than the gain-dispersion parameter $T_R = \gamma_R^{-1} \approx 3$ ps, we can approximate gain profile by the function

$$G_R(\omega) \approx \frac{\hat{g}_R}{2}\frac{\gamma_R}{\gamma_R - i\omega} \approx \frac{\hat{g}_R}{2}\left(1 + \frac{i\omega}{\gamma_R} - \frac{\omega^2}{\gamma_R^2}\right).$$

Using this result to convert Eq. (1) into the time domain, we arrive at the following equation for signal envelope $A_s(z,t)$:

$$\frac{\partial A_s}{\partial z} + \left[\beta_{1s} + \frac{1}{2}\hat{g}_R T_R I_p(z)\right]\frac{\partial A_s}{\partial t} + \frac{1}{2}\left[i\beta_{2s} + \hat{g}_R T_R^2 I_p(z)\right]\frac{\partial^2 A_s}{\partial t^2}$$
$$= \left[-\frac{\alpha_s}{2} + \left(\frac{\hat{g}_R - 2\beta_s}{2} + 2i\gamma_s\right)I_p(z) - \left(\frac{\xi_r}{2} + i\xi_i\right)I_p^2(z)\right]A_s. \quad (3)$$

This equation should be solved together with boundary condition $A_s(0,t) = f(t)$, where $f(t)$ is the input pulse profile. Once the solution is found, the evolution of signal power inside the silicon Raman amplifier (SRA) of a given effective mode area A_{eff} is given by $P_s(z,t) = |A_s(z,t)|^2 A_{\text{eff}}$.

2.2. Propagation equation for the CW pump and its solution

We start by considering the simplest situation in which a single-pass SRA of length L is pumped using a CW pump of intensity I_0. In the undepleted-pump approximation, the attenuation of pump can be found from the equation

$$\pm\frac{1}{I_p(z)}\frac{\mathrm{d}I_p(z)}{\mathrm{d}z} = -\alpha_p - \beta_p I_p(z) - \xi_p I_p^2(z), \quad (4)$$

where α_p is the linear-loss coefficient at pump wavelength and $\xi_p = (\omega_s/\omega_p)^2\xi_r$. The plus (minus) sign applies to forward-pumped (backward-pumped) SRA.

#131277 - $15.00 USD Received 7 Jul 2010; revised 11 Aug 2010; accepted 11 Aug 2010; published 12 Aug 2010

Equation (4) has an explicit solution in the regime of weak TPA, applicable when $\beta_p^2 \ll \alpha_p \xi_p$ [16, 46]. Assuming this to be the case, we obtain the pump intensity in the form

$$I_p^{\pm}(z) = \frac{I_0 \exp[\mp\alpha_p(z-\delta_{\pm})]}{\sqrt{1+I_0^2(\xi_p/\alpha_p)\{1-\exp[\mp 2\alpha_p(z-\delta_{\pm})]\}}}, \tag{5}$$

where $\delta_{\pm} = L(1\mp 1)/2$ specifies the location of pump launching. Notice that $I_p^+(z) = I_p^-(L-z)$; that is, the intensity profiles of two pumps propagating in opposite directions are the mirror image of each other around the amplifier's center. For compactness, we omit the superscripts $\pm$ in all the functions of propagation distance in the rest of this paper, unless necessary for clarity.

Using Eq. (5), we can introduce an effective propagation length as [32, 44]

$$L_{\text{eff}}(z) = \frac{1}{I_0}\int_0^z I_p(z')\,\mathrm{d}z' = \pm\frac{\tan^{-1}[I_p(0)\sqrt{\xi_p/\alpha_p}] - \tan^{-1}[I_p(z)\sqrt{\xi_p/\alpha_p}]}{I_0\sqrt{\alpha_p\xi_p}}. \tag{6}$$

Equations (5) and (6) show that the effective propagation length in a forward-pumped SRA exceeds that in a backward-pumped SRA for $z < L$, all other factors being equal. However, the effective length of SRA, $L_{\text{eff}}(L)$, is the same for both pumping configurations.

The situation becomes more complex in the case of bidirectional pumping. This pumping geometry may be preferable to the unidirectional pumping in long SRAs, if it is required to get the maximal gain, and in short SRAs, if the object is to have the longest pulse delay. The intensities of forward- and backward-traveling waves inside the SRA pumped from both ends obey the equations

$$\pm\frac{1}{I_{\pm}}\frac{\mathrm{d}I_{\pm}}{\mathrm{d}z} \approx -\alpha_p - \xi_p\left(I_+^2 + I_-^2 + 4I_+I_-\right).$$

These equations are readily integrated to obtain [46]

$$I_+(z) = \sqrt{a\coth(qz+C_2) - b}, \quad I_-(z) = C_1/I_+(z),$$

where $a = q/(2\xi_p)$, $b = 2C_1 + \alpha_p/(2\xi_p)$, and $q = \sqrt{(\alpha_p + 2\xi_p C_1)(\alpha_p + 6\xi_p C_1)}$. Ignoring, as before, the reflections of pumps from amplifier facets, we can find the integration constants C_1 and C_2 from the system

$$I_+(0) = \eta I_0, \quad I_-(L) = (1-\eta)I_0,$$

where η determines the amount of the total pump intensity launched at $z = 0$.

The effective propagation length in the bidirectionally pumped SRA is defined as

$$\mathscr{L}_{\text{eff}}(\eta, z) = \frac{1}{I_0}\int_0^z [I_+(z') + I_-(z')]\,\mathrm{d}z' = \frac{T(0) - T(z)}{I_0\left(\sqrt{b+a} + \sqrt{b-a}\right)\xi_p},$$

where

$$T(z) = \tan^{-1}\left(\frac{I_+(z)}{\sqrt{b+a}}\right) + \tan^{-1}\left(\frac{I_+(z)}{\sqrt{b-a}}\right).$$

It is easy to see that, since the pump is undepleted, the effective length exhibits the property $\mathscr{L}_{\text{eff}}(\eta, L) = \mathscr{L}_{\text{eff}}(1-\eta, L)$. Thus, values of η's in the range $0.5 \le \eta \le 1$ provide all possible signal gains.

Figure 2 shows the effective length of a typical, 1-cm-long SRA with 100, 85, and 50% of forward pumping (left panel). One can see that bidirectional pumping may increase the

#131277 - $15.00 USD Received 7 Jul 2010; revised 11 Aug 2010; accepted 11 Aug 2010; published 12 Aug 2010

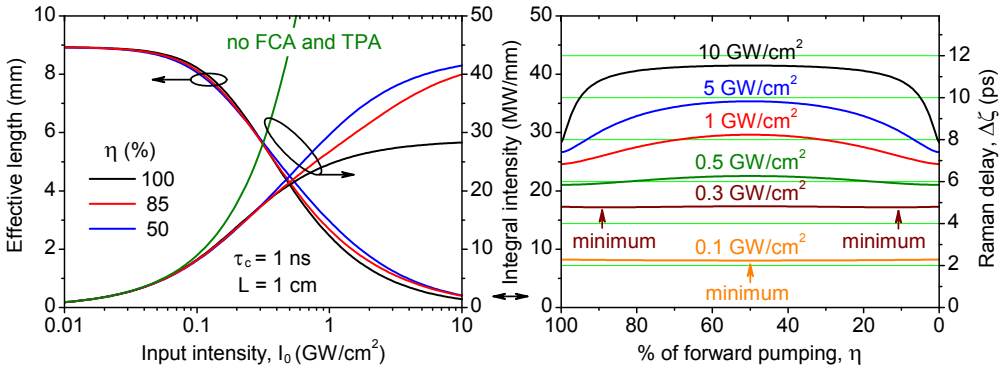

Fig. 2. Effective length of bidirectionally pumped, 1-cm-long SRA (left panel) and integral intensity (left and right panels) for different contributions of the forward pumping. The green curve on the left panel shows, for comparison, the case of a SRA without nonlinear losses. In the calculations, we used $\lambda_p = 1434$ nm, $\alpha_p = 1$ dB/cm, and $\tau_c = 1$ ns.

effective length of the amplifier by reducing nonlinear losses at high input intensities, but it can also reduce it by introducing cross-TPA when pump intensities are low. The variations in the effective length with I_0 and η result in similar variations of the intensity integral, $I_0\mathscr{L}_{\rm eff}(\eta, L)$, shown in both panels of Fig. 2. As we shall see later, the intensity integral of the pump is crucial for the Raman delay experienced by the signal from Raman-gain dispersion (see right panel in Fig. 2).

2.3. *Analytic solution of the propagation equation for signal pulses*

The linear partial differential equation (3) can be solved in quadratures for an arbitrary intensity profile of a CW pump and arbitrary signal envelope $f(t)$. We first consider unidirectional pumping and obtain a general closed-form solution in this case by using Eqs. (5) and (6).

Introducing the generalized retarded time,

$$\zeta(z,t) = t - \beta_{1s} z - \frac{1}{2}\hat{g}_R T_R \int_0^z I_p(z')\,\mathrm{d}z' = \tau(z,t) - \frac{1}{2}\hat{g}_R T_R I_0 L_{\rm eff}(z), \tag{7}$$

where $\tau(z,t) = t - \beta_{1s} z$, we can rewrite Eq. (3) in the form

$$\frac{\partial A_s}{\partial z} + \frac{\mathscr{B}(z)}{2}\frac{\partial^2 A_s}{\partial \zeta^2} = \frac{\mathscr{G}(z)}{2} A_s, \tag{8}$$

where $\mathscr{B}(z)$ and $\mathscr{G}(z)$ are the functions of z only.

The solution of Eq. (8) can be factorized in the form

$$A_s(z,\zeta) = a[\chi(z),\zeta]\exp[\psi(z)/2], \tag{9}$$

where

$$\chi(z) = \int_0^z \mathscr{B}(z')\,\mathrm{d}z' = \hat{g}_R T_R^2 I_0 L_{\rm eff}(z) + i\beta_{2s} z, \tag{10}$$

$$\psi(z) = \int_0^z \mathscr{G}(z')\,\mathrm{d}z' = -\alpha_s z + (\hat{g}_R - 2\beta_s + 4i\gamma_s) I_0 L_{\rm eff}(z) - (1 + 2i\xi_i/\xi_r) Q(z), \tag{11}$$

$$Q(z) = \xi_r \int_0^z I_p^2(z')\,\mathrm{d}z' = \frac{\omega_p^2}{\omega_s^2}\left(\pm \ln\frac{I_p(0)}{I_p(z)} - \alpha_p z\right).$$

#131277 - $15.00 USD Received 7 Jul 2010; revised 11 Aug 2010; accepted 11 Aug 2010; published 12 Aug 2010

Substituting Eq. (9) in Eq. (8), the function $a(\chi,\zeta)$ is found to obey the diffusion equation

$$2\frac{\partial a}{\partial \chi}=\frac{\partial^2 a}{\partial \zeta^2},$$

whose solution with the boundary condition $a(0,\tau)=f(\tau)$ is given by [47]

$$a(\chi,\tau)=\frac{1}{\sqrt{2\pi\chi}}\int_{-\infty}^{+\infty} f(\tau+u)\exp\left(-\frac{u^2}{2\chi}\right)\mathrm{d}u. \tag{12}$$

Since $\mathrm{Re}\,\chi>0$, this integral converges for all physically admissible pulse profiles $f(\tau)$. Equations (7) and (9)–(12) allows one to find the evolution of signal envelope $A_s(z,t)$ for an arbitrary input profile $f(t)$; they constitute one of the major results of our paper.

The situation of bidirectional pumping can be described in a similar fashion. To apply the above solution in this case, one needs to replace $L_{\mathrm{eff}}(z)$ by $\mathscr{L}_{\mathrm{eff}}(\eta,z)$ and use

$$Q(z)=\xi_r\left[\frac{C_1}{2q}\left(K_+\ln\frac{G_+(z)}{G_+(0)}-K_-\ln\frac{G_-(z)}{G_-(0)}\right)+\frac{a}{q}\ln\left(\frac{\sinh(qz+C_2)}{\sinh C_2}\frac{\eta^2 I_0^2}{I_+^2(z)}\right)-bz\right]$$

with $K_\pm=4-\sqrt{(b\mp a)/(b\pm a)}$ and $G_\pm(z)=\coth(qz+C_2)\pm 1$.

3. Raman amplification in SRAs based on our analytic solution

3.1. General features of Raman amplification for picosecond pulses

Several general conclusions can be drawn by examining the structure of our analytic solution, even without specifying a particular shape of the signal pulse. First, since the values of the functions ζ, χ, and ψ at the amplifier output $z=L$ are the same for forward-traveling and backward-traveling pumps, *the gain provided by a unidirectionally pumped SRA does not depend on the pumping direction in the undepleted-pump regime.* In other words, even though the dynamics of a signal pulse inside a SRA differ for the forward- and backward-pumping configurations, the output signal pulse profiles do not. The backward-pumping geometry is preferable though, as it enables better noise performance by lowering noise transfer from the pump to the signal [48].

Second, Eq. (12) shows that a signal pulse with initially symmetric envelope $[f(t)=f(-t)]$ preserves its temporal symmetry as it propagates through the amplifier. The spatial symmetry of the pulse still breaks inside the waveguide, in the sense that the pulse profile is not symmetric around the point of its peak intensity.

Third, the delay of signal pulse—accumulated over amplifier length owing to the effect of Raman dispersion—is proportional to the integral of the pump intensity, $\int_0^L I_p(z)\,dz$. In the case of unidirectional pumping, this slow-light contribution is given by the remarkably simple expression

$$\Delta\zeta=\frac{1}{2}\hat{g}_R T_R I_0 L_{\mathrm{eff}}(L).$$

The delays calculated when a 1.434-μm pump is used to amplify a 1.55-μm signal pulse are shown on the right scale in Fig. 2. Since, according to Eq. (6), the product $I_0 L_{\mathrm{eff}}(L)$ saturates with both incident pump intensity and amplifier length, the maximum delay produced by a CW pump of intensity I_0 is given by

$$\Delta\zeta_{\max}(I_0)=\frac{1}{2}\hat{g}_R T_R\frac{\tan^{-1}\left(I_0\sqrt{\xi_p/\alpha_p}\right)}{\sqrt{\alpha_p\xi_p}}.$$

#131277 - $15.00 USD Received 7 Jul 2010; revised 11 Aug 2010; accepted 11 Aug 2010; published 12 Aug 2010

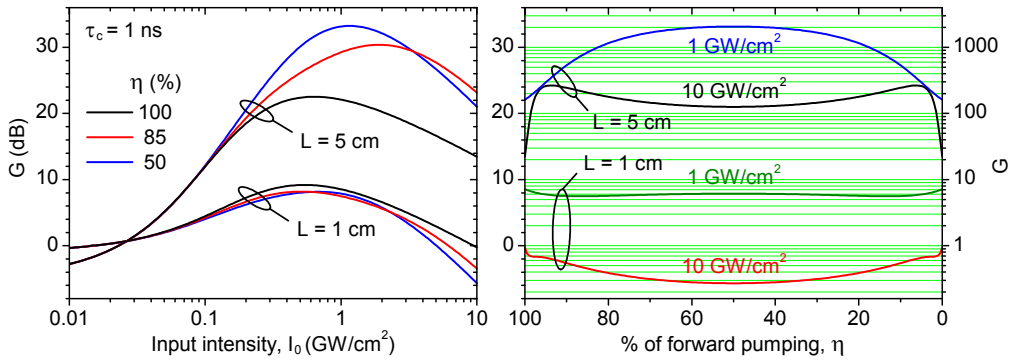

Fig. 3. Evolution of maximum signal gain, $G = \exp[\psi'(L)]$, in two bidirectionally pumped SRAs for different contributions of forward pumping. The parameters' values are: $\lambda_p = 1.434\ \mu$m, $\lambda_s = 1.55\ \mu$m, $\alpha_p = \alpha_s = 1$ dB/cm, $\beta_p = \beta_s = 0.5$ cm/GW, and $\tau_c = 1$ ns.

Since the maximum value of $\tan^{-1} x$ is $\pi/2$ in the limit $x \to \infty$, it is evident that FCA imposes a fundamental upper limit on the Raman delay time given by

$$\Delta T = \frac{\pi}{4} \frac{\hat{g}_R T_R}{\sqrt{\alpha_p \xi_p}}.$$

For example, if $\alpha_p \xi_p = 20\beta_p^2 = 5\ (\text{cm/GW})^2$ and $g_R = 20$ cm/GW, then $\Delta T \approx 7T_R \approx 21$ ps. Hence, a relatively narrow bandwidth of the Raman gain spectrum allows one to create substantial tunable delays, even for 10-ps signal pulses [38,45]. It is important to note that ΔT increases with decreasing values of the free-carrier lifetime and linear-loss coefficient as $(\alpha_p \tau_c)^{-1/2}$. In the absence of FCA ($\tau_c = 0$), the intensity integral does not saturate (see Section 1), and pulse delays can grow unrestrictedly with increasing pump power.

Fourth, the evolution of pulse energy is governed only by the real parts of the functions $\chi(z)$ and $\psi(z)$,

$$\chi'(z) = \hat{g}_R T_R^2 I_0 L_{\text{eff}}(z), \quad \psi'(z) = -\alpha_s z + (\hat{g}_R - 2\beta_s) I_0 L_{\text{eff}}(z) - Q(z).$$

In particular, for real-valued envelopes $f(\tau)$, the total energy of the pulse is given by (see the Appendix)

$$W(z) = A_{\text{eff}} \exp[\psi'(z)] \int_{-\infty}^{+\infty} a[2\chi'(z), \tau] f(\tau)\, \mathrm{d}\tau. \tag{13}$$

This integral allows for a finite Raman response time; if T_R formally tends to zero, the integral approaches its maximum value W_0/A_{eff}, W_0 being the energy of the input pulse. For this reason, the quantity $G = \exp[\psi'(L)]$ can be identified as the maximum signal gain provided by SRA in the limit of the instantaneous Raman response. The dependance of G on the incident pump intensity and its fraction launched in the forward direction, is shown in Fig. 3. It can be seen that, at moderate pump powers, the maximum signal gain begins to decrease as the effective length increases (see left panels in Figs. 2 and 3), thereby restricting the possibility of achieving long delays and strong amplification simultaneously.

It is worthwhile to note that, if $\Delta\zeta \ll L/c$ and the slow-light effects can be ignored, Eq. (3) reduces to Eq. (1) from Ref. [38], with $|E_p|^2 \gg |E_s|^2$. Thus, our solution not only covers and extends the results of Ref. [38], but it also has the form that is much more favorable for the analysis.

#131277 - $15.00 USD Received 7 Jul 2010; revised 11 Aug 2010; accepted 11 Aug 2010; published 12 Aug 2010

3.2. *Evolution of pulse energy and envelope for three specific pulse shapes*

To illustrate the application of the general solution (9)–(12), we consider three unchirped input pulses with energy W_0 and FWHM τ_0,

$$f_1(\tau)=\frac{\varpi_1}{\pi^{1/4}}\exp\left(-\frac{\tau^2}{2\tau_1^2}\right),\quad f_2(\tau)=\frac{\varpi_2}{\sqrt{2}}\exp\left(-\frac{|\tau|}{2\tau_2}\right),\quad f_3(\tau)=\varpi_3\sqrt{\frac{2}{\pi}}\frac{\tau_3^2}{\tau^2+\tau_3^2},$$

where $\varpi_j=\sqrt{W_0/(\tau_j A_{\rm eff})}$, $\tau_1=\tau_0/(2\sqrt{\ln 2})$, $\tau_2=\tau_0/(2\ln 2)$, and $\tau_3=\tau_0/\left(2\sqrt{2^{1/2}-1}\right)$. For these pulses, the integral in Eq. (12) has the following closed forms:

$$a_1(\chi,\tau)=\frac{\varpi_1}{\pi^{1/4}}\frac{\tau_1}{\sqrt{\tau_1^2+\chi}}\exp\left(-\frac{\tau^2}{2(\tau_1^2+\chi)}\right),$$

$$a_2(\chi,\tau)=\frac{\varpi_2}{2\sqrt{2}}\left[\operatorname{erfc}\left(\frac{\chi+2\tau_2\tau}{2\tau_2\sqrt{2\chi}}\right)e^{\tau/(2\tau_2)}+\operatorname{erfc}\left(\frac{\chi-2\tau_2\tau}{2\tau_2\sqrt{2\chi}}\right)e^{-\tau/(2\tau_2)}\right]e^{\chi/(8\tau_2^2)},$$

$$a_3(\chi,\tau)=\varpi_3\frac{\tau_3}{2\sqrt{\chi}}\left[\operatorname{erfc}\left(\frac{\tau_3+i\tau}{\sqrt{2\chi}}\right)e^{(\tau_3+i\tau)^2/(2\chi)}+\operatorname{erfc}\left(\frac{\tau_3-i\tau}{\sqrt{2\chi}}\right)e^{(\tau_3-i\tau)^2/(2\chi)}\right],$$

where $\operatorname{erfc}x$ is the complementary error function. Using Eq. (13), it is easy to show that the energies of the three pulses evolve along the SRA length as

$$W_1(z)=W_0\frac{\tau_1}{\sqrt{\tau_1^2+\chi'}}\exp\psi',\quad W_2(z)=W_0\operatorname{erfc}\left(\frac{\sqrt{\chi'}}{2\tau_2}\right)\exp\left(\frac{\chi'}{4\tau_2^2}+\psi'\right),$$

$$W_3(z)=W_0\frac{\tau_3^2}{\sqrt{\pi\chi'}}\exp\psi'\int_{-\infty}^{+\infty}\operatorname{erfc}\left(\frac{\tau_3+i\tau}{2\sqrt{\chi'}}\right)\frac{\exp[(\tau_3+i\tau)^2/(4\chi')]}{\tau^2+\tau_3^2}\,d\tau.$$

We note that the SRS-induced energy enhancement for two of these pulses depends on a single dimensionless parameter $\sqrt{\chi'}/(2\tau_0)$.

Our analytic solution shows that while a Gaussian pulse preserves its temporal profile throughout the amplifier length, the exponential and Lorentzian pulses do not. This is a well known feature of linear systems, which in our case holds owing to the adopted approximation for the Raman gain profile. As a result, the intensity and nonlinear phase shift can be expressed using elementary functions only for a Gaussian pulse and are given by

$$I(z,\zeta)=|A_s(z,\zeta)|^2=\frac{\varpi_1^2}{\sqrt{\pi}}\frac{\tau_1^2}{\sqrt{(\tau_1^2+\chi')^2+(\chi'')^2}}\exp\left(-\frac{(\tau_1^2+\chi')\zeta^2}{(\tau_1^2+\chi')^2+(\chi'')^2}+\psi'\right),\quad(14)$$

$$\phi_{\rm NL}(z,\zeta)=\operatorname{Arg}[A_s(z,\zeta)]=\mathfrak{S}\left\{\frac{1}{2}\left[\frac{\chi''\zeta^2}{(\tau_1^2+\chi')^2+(\chi'')^2}-\tan^{-1}\left(\frac{\chi''}{\tau_1^2+\chi'}\right)+\psi''\right]\right\},\quad(15)$$

where $\chi''=\operatorname{Im}\chi$ and $\psi''=\operatorname{Im}\psi$. The operator $\mathfrak{S}(x)=x-2\pi\langle x/(2\pi)\rangle$, where $\langle a\rangle$ denotes the integer closest to a, shifts the phase into the interval $-\pi\le\phi_{\rm NL}(z,\zeta)\le\pi$. Since the propagation of a Gaussian pulse is of practical interest, we consider it in more detail.

3.3. *Soliton-like propagation of chirped Gaussian pulses in SRAs*

Equation (14) shows that an unchirped Gaussian pulse always spreads, due to both group-velocity dispersion and Raman dispersion. However, if the input pulse has a sufficiently large linear chirp σ, it may undergo a compression stage due to its increased spectral bandwidth [38].

#131277 - $15.00 USD Received 7 Jul 2010; revised 11 Aug 2010; accepted 11 Aug 2010; published 12 Aug 2010

This interesting phenomena can be used to realize gain-assisted soliton-like propagation, such that both the amplitude and width of the signal pulse are restored to their initial values at the end of the amplifier.

To find the parameters of the soliton-like pulse, we first use our analytic solution to find the temporal width and the peak intensity of a chirped Gaussian pulse at the output end of the SRA:

$$T_\sigma = \left(\frac{(\tau_1^2 + \chi' + \sigma\chi'')^2 + (\chi'' - \sigma\chi')^2}{\tau_1^2 + (1+\sigma^2)\chi'} \right)^{1/2}, \quad I_\sigma \propto \frac{\tau_1^2 \exp(\psi')}{T_\sigma \sqrt{\tau_1^2 + (1+\sigma^2)\chi'}}.$$

The first equation shows that it is always possible to find a chirp that results in $T_\sigma = \tau_1$ at the end of the amplifier. The required chirp obeys the equation

$$(\sigma^2 - 1)\chi'\tau_1^2 - 2\sigma\chi''\tau_1^2 = (1+\sigma^2)|\chi|^2. \tag{16}$$

At the same time, since equal amplitudes for the input and output pulses are also required, another condition should be satisfied,

$$\tau_1^2(G^2 - 1) = (1+\sigma^2)\chi'. \tag{17}$$

As the chirp results in additional losses, the soliton-like propagation is only possible in the presence of a net gain ($G > 1$).

Solving Eqs. (16) and (17), where all the functions are considered at $z = L$, we obtain

$$\sigma = \frac{\chi'' \pm |\chi| G}{\chi'} \approx \pm G, \tag{18}$$

$$\tau_1 = \frac{|\chi|}{\sqrt{\chi'}} \left(\frac{G^2 \pm 2(\chi''/|\chi|)G + 1}{G^2 - 1} \right)^{1/2} \approx \sqrt{\chi' \coth \psi'}, \tag{19}$$

where we took into account that $\chi' \approx |\chi| \gg \chi''$ for typical operation conditions of SRAs. The values of the chirp enabling soliton-like propagation for 1- and 5-cm-long SRAs can be inferred from Fig. 3, where G is plotted as a function of pump intensity I_0. Using σ from Eq. (18) and τ_1 from Eq. (19), the energy of the soliton-like pulse is found to evolve along the SRA length as

$$W_s(z) = \frac{W_0 \exp[\psi'(z)]}{\sqrt{1 + (G^2 - 1)\chi'(z)/\chi'(L)}}.$$

4. Numerical examples and discussion

For a numerical example illustrating the analytic results obtained in the previous section, we consider the pump at 1.434 μm and assume that a signal pulse at 1.55 μm propagates in the form of a TE mode with the effective area $A_{\text{eff}} = 0.18\ \mu\text{m}^2$. Assuming propagation in the regime of normal dispersion characterized by the parameter $D = -1\,\text{ps}/(\text{m} \times \text{nm})$, we find β_{2s} using $\beta_{2s} = -(2\pi c/\omega_s^2)D$. We also use parameter values $\alpha_s = \alpha_p = 1\ \text{dB/cm}$, $\beta_p = \beta_s = 0.5\ \text{cm/GW}$, and $g_R = 20\ \text{cm/GW}$.

Figure 4 shows how the intensity profiles of (1) Gaussian, (2) exponential, and (3) Lorentzian pulses change in a forward-pumped SRA. The initial energy (1 pJ) and initial width ($\tau_0 = 10$ ps) are the same for all three pulses. One can see that the pulses exhibit substantial broadening, dominated by the Raman dispersion. Specifically, the FWHM of the Gaussian pulse increases according to the equation $T_G(z) \approx \tau_0 \left[1 + 2T_R \Delta\zeta(z)/\tau_1^2\right]^{1/2}$, which gives $T_G(L)/\tau_0 \approx 1.5$. Since

#131277 - $15.00 USD Received 7 Jul 2010; revised 11 Aug 2010; accepted 11 Aug 2010; published 12 Aug 2010

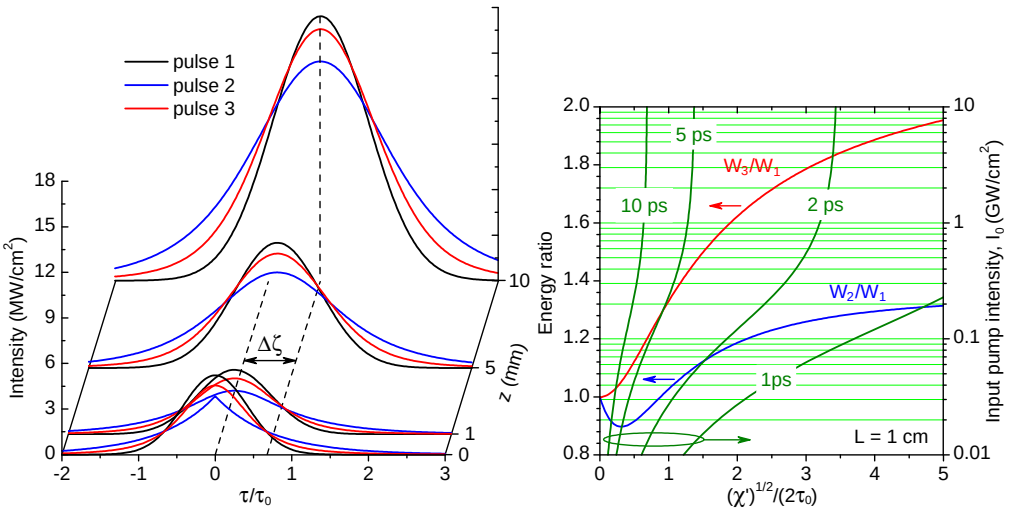

Fig. 4. Evolution of three 10-ps pulses with different temporal envelopes (left panel) and relative energies of the pulses as a function of pump intensity for different values of τ_0 (right panel); $W_0 = 1$ fJ and $I_0 = 1$ GW/cm^2 in the left panel; $\eta = 100\%$ and $\tau_c = 1$ ns for both panels. Other parameters are given in the text.

the exponential and Lorentzian pulses have wider spectra than that of a Gaussian pulse ($\tau_1 > \tau_2 > \tau_3$), they broaden faster. The other effect of Raman dispersion is the delay of all three pulses by $\Delta\zeta \approx 6.8$ ps (see Fig. 2) at the output of SRA. The delay is proportional to the Raman gain coefficient and can be several times higher, if the largest reported value of g_R is used for numerical simulations [49]. The right panel in Fig. 4 shows the energy enhancement of exponential and Lorentzian pulses at the end of 1-cm-long amplifier. As seen from this panel, the Lorentzian pulse always gains more energy than a Gaussian pulse of the same width, irrespective of the pump intensity. The energy of exponential pulse is smaller than that of a Gaussian pulse for $\tau_0 > 10$ ps, but may exceed it at high pump powers, when $\tau_0 \lesssim 5$ ps. Recall that the analytical solution becomes less accurate as the width of pulse approaches the gain-dispersion parameter $T_R \approx 3$ ps.

The dynamics of a soliton-like, chirped Gaussian pulse is presented in Figs. 5(a) and 5(b) for forward and backward pumping, respectively. When the pulse enters the SRA, it experiences strong absorption [see Fig. 5(d)] and temporal compression, regardless of the pumping configuration. The difference in profile evolution for the two pumping directions is related to the different rates of FCA. In the case of forward pumping, losses caused by an increased signal bandwidth and a large FCA act together near the front end, leading to a considerable decay in the peak intensity. In a backward-pumped SRA, FCA induces net loss just near the output, and the compression is accompanied with a growth in the peak power. After the absorption stage, signal starts accumulating energy and broadens until it acquires its initial peak intensity and width at the end of the amplifier. The value of chirp in Figs. 5(a) and 5(b) is approximately equal to 7.1 (see Fig. 3). The width of the pulse, $\tau_0 \approx 10.9$ ps, can be found from Fig. 5(c). As seen from this figure, FWHM of the soliton-like pulse is larger in bidirectionally pumped amplifiers and strongly depends on the pump intensity.

#131277 - $15.00 USD Received 7 Jul 2010; revised 11 Aug 2010; accepted 11 Aug 2010; published 12 Aug 2010

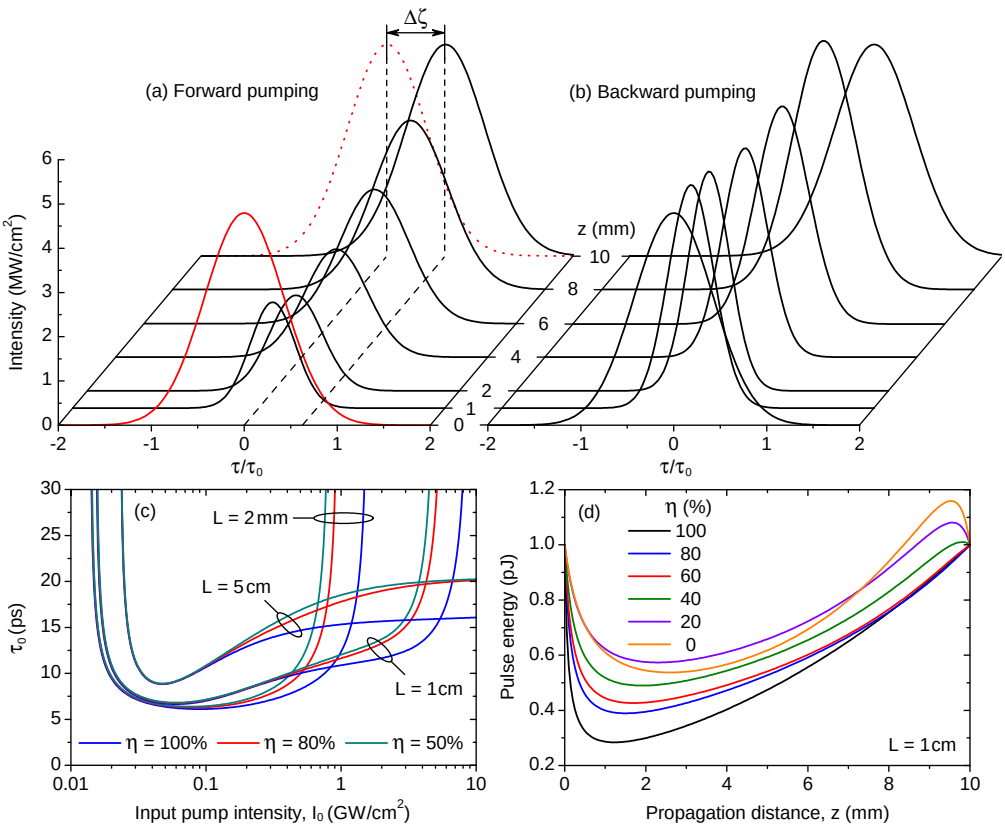

Fig. 5. Soliton-like evolution of a Gaussian pulse in (a) forward- and (b) backward-pumped, 1-cm-long SRA. (c) Input FWHM of the soliton-like pulse for 0.2-, 1-, and 5-cm-long SRAs. (d) Evolution of pulse energy as the amount of forward pumping is varied from 100% to zero. $I_0 = 1$ GW/cm^2 in panels (a), (b), and (d); $W_0 = 1$ fJ and $\tau_c = 1$ ns for all panels. Other parameters are given in the text.

5. Conclusions

In this work, we presented—for the first time to the best of our knowledge—an exact analytical solution for the amplification of picosecond pulses (with an arbitrary shape) in a CW-pumped SRA. The solution is applicable in a wide range of practical situations in which the undepleted-pump approximation and the parabolic fit for the Raman gain profile remain valid. With the obtained solution, we analyzed the specific features of pulse amplification in unidirectionally and bidirectionally pumped SRAs. In particular, we found an analytic expression for the maximum Raman-dispersion-induced group delay (a slow-light effect) that can be achieved for a given pump intensity. We also analyzed how the envelopes and energies of Gaussian, exponential, and Lorentzian pulses evolve during the amplification process. The analysis reveals that a Gaussian pulse—which preserves its shape during Raman amplification—can demonstrate a soliton-type behavior if it is appropriately chirped at the input end. The linear chirp and temporal width, required to realize such soliton-like propagation, are derived analytically. Our solution provides a clear insight into the Raman amplification process of optical pulses in silicon waveguides, and offers a simple analytical tool that may prove essential for optimization of the amplifier performance.

#131277 - $15.00 USD Received 7 Jul 2010; revised 11 Aug 2010; accepted 11 Aug 2010; published 12 Aug 2010

Appendix

According to Eqs. (9) and (12), the energy of signal pulse, $W(z) = A_{\rm eff}\int_{-\infty}^{+\infty}|A_s(z,\tau)|^2\,{\rm d}\tau$, is proportional to the integral

$$\mathscr{I}(\chi) = \frac{1}{2\pi|\chi|}\int\limits_{-\infty}^{+\infty}{\rm d}\tau\int\limits_{-\infty}^{+\infty}{\rm d}u\int\limits_{-\infty}^{+\infty}{\rm d}u'\,f(\tau+u)[f(\tau+u')]^*\exp\left(-\frac{u^2}{2\chi}-\frac{u'^2}{2\chi^*}\right),$$

where an asterisk denotes complex conjugation. Introducing new variables, $q=\tau+u$ and $N=u-u'$, we can evaluate this integral as

$$\begin{aligned}\mathscr{I}(\chi) &= \frac{1}{2\pi|\chi|}\int\limits_{-\infty}^{+\infty}{\rm d}q\,f(q)\int\limits_{-\infty}^{+\infty}{\rm d}N\,[f(q-N)]^*\exp\left(-\frac{N^2}{2\chi}\right)\int\limits_{-\infty}^{+\infty}{\rm d}u'\exp\left(-\frac{\chi' u'^2}{|\chi|^2}-\frac{Nu'}{\chi}\right)\\ &= \frac{1}{\sqrt{4\pi\chi'}}\int\limits_{-\infty}^{+\infty}{\rm d}q\,f(q)\int\limits_{-\infty}^{+\infty}{\rm d}N\,[f(q-N)]^*\exp\left(-\frac{N^2}{4\chi'}\right)=\int\limits_{-\infty}^{+\infty}{\rm d}q\,f(q)[a(2\chi',q)]^*.\end{aligned}$$

For $f(\tau)=f^*(\tau)$, the last integral coincides with the integral in Eq. (13).

Acknowledgments

The work of I. D. Rukhlenko, M. Premaratne, and G. P. Agrawal was sponsored by the Australian Research Council (ARC) through its Discovery Grant scheme under grant DP0877232. The work of G. P. Agrawal was also supported by the NSF Award ECCS-0801772. The work of I. L. Garanovich and A. A. Sukhorukov was sponsored by the ARC through its Discovery and Center of Excellence programs.

#131277 - $15.00 USD Received 7 Jul 2010; revised 11 Aug 2010; accepted 11 Aug 2010; published 12 Aug 2010